

# Dipping Our Toes in the Water: First Models of GD-1 as a Stream

A. Bowden<sup>1\*</sup>, V. Belokurov<sup>1</sup>, N.W. Evans<sup>1</sup>

<sup>1</sup>*Institute of Astronomy, University of Cambridge, Madingley Road, Cambridge, CB3 0HA, UK*

4 March 2022

## ABSTRACT

We present a model for producing tidal streams from disrupting progenitors in arbitrary potentials, utilizing the idea that the majority of stars escape from the progenitor’s two Lagrange points. The method involves releasing test particles at the Lagrange points as the satellite orbits the host and dynamically evolving them in the potential of both host and progenitor. The method is sufficiently fast to allow large-dimensional parameter exploration using Monte Carlo methods. We provide the first direct modelling of 6-D stream observations – assuming a stream rather than an orbit – by applying our methods to GD-1. This is a kinematically cold stream spanning  $60^\circ$  of the sky and residing in the outer Galaxy  $\approx 15$  kpc distant from the centre. We assume the stream moves in a flattened logarithmic potential characterised by an asymptotic circular velocity  $v_0$  and a flattening  $q$ . We recover values of normalisation  $v_0 = 227.2^{+15.6}_{-18.2}$  kms<sup>−1</sup> and flattening  $q = 0.91^{+0.04}_{-0.1}$ , if the stream is assumed to be leading, and  $v_0 = 226.5^{+17.9}_{-17.0}$  kms<sup>−1</sup>,  $q = 0.90^{+0.05}_{-0.09}$ , if it is assumed to be trailing. This can be compared to the values  $v_0 = 224 \pm 13$  kms<sup>−1</sup> and  $q = 0.87^{+0.07}_{-0.04}$  obtained by Koposov et al (2010) using the simpler technique of orbit fitting. Although there are differences between stream and orbit fitting, we conclude that orbit fitting can provide accurate results given the current quality of the data, at least for this kinematically cold stream in this logarithmic model of the Galaxy.

**Key words:** galaxies: fundamental parameters – galaxies: haloes – galaxies: kinematics and dynamics

## 1 INTRODUCTION

As satellite galaxies and globular clusters orbit their host galaxy, they experience strong tidal forces. Stars are stripped from the satellite onto orbits that are close to that of the progenitor, forming tidal streams (e.g., Johnston et al. 1995, Fellhauer et al. 2006). Such streams contain information about the potential in which they form, allowing us to probe the structure of our Galaxy.

The Sagittarius (Sgr) dwarf galaxy provides the most famous example of a tidally disrupting system. Its leading and trailing tails have now been traced across most of the sky (e.g., Koposov et al. 2012, Belokurov et al. 2014). The Sgr stream is unusually complex, probably because its progenitor was a dwarf irregular comparable in mass to the Small Magellanic Cloud (Niederste-Ostholt et al. 2010). More numerous than such thick streams are thin and wispy tidal tails, such as the extended trail of debris from the globular cluster Pal 5 found in Sloan Digital Sky Survey (SDSS) commissioning data (Odenkirchen et al. 2003). In fact, the high quality photometric data of the SDSS proved a gold-mine for the discovery of stellar streams. Amongst the many discoveries were the tidal tails of NGC 5466 (Belokurov et al. 2005, Grillmair & Johnson 2006), the Orphan Stream (Grillmair 2006, Belokurov et al. 2007),

the GD-1 Stream (Grillmair & Dionatos 2006) and the Acheron, Cocytos, Lethe and Styx streams (Grillmair 2009). These kinematically cold streams are derived from less massive progenitors than the Sgr, and hence are easier to understand and model.

An appealingly simple assumption is to model the stream as an orbit in an underlying potential (e.g., Jin & Lynden-Bell 2007, Willett et al. 2010, Newberg et al. 2011, Lux et al. 2013, Deg & Widrow 2014). Koposov, Hogg & Rix (2010, hereafter K10) used just this method to model the GD-1 tidal stream in a flattened logarithmic potential. At first sight, this seems a reasonable assumption, particularly for a narrow and long stream such as GD-1. However, doubts were soon raised by a number of investigators. First, Eyre & Binney (2011) argued that streams in realistic potentials are poorly represented by single orbits. Then, Sanders & Binney (2013a,b) also showed that the misalignment between a stream and an orbit can be substantial and cautioned against the practice of orbit fitting even for narrow streams. They developed a formalism for stream fitting in action-angle coordinates and tested it on mock data.

There have been a number of other recent investigations into the problem of fitting streams to mock data extracted from simulations. Bovy (2014) provided a framework for computing the evolution of streams in action-angle coordinates, as well as for deriving the probability distribution for data analysis of the stream stars. Bonaca et al. (2014) inserted streams into a resimulation of the Via

\* E-mail: adb61,vasily,nwe@ast.cam.ac.uk

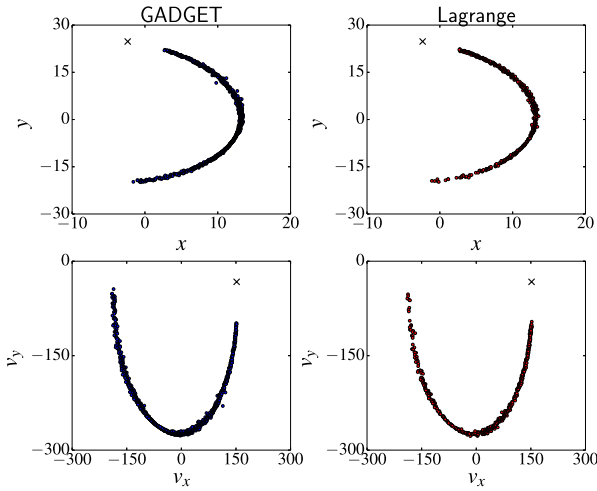


**Figure 1.** Comparison of a trailing stream produced via GADGET N-body simulations to one produced with a Lagrange point stripping method in both position and velocity. The satellite location is represented by a black cross. The broad properties of the stream in both position and velocity space are well reproduced.

Lactea II simulation, created mock observations and fitted them to constrain the host galaxy mass and to estimate the biases. Finally, Price-Whelan et al. (2014) developed a novel method of estimating the potential using a small number of stream stars without explicitly modelling the stream. However, none of these authors applied their methods to actual observational data on a stream to demonstrate unambiguously that orbit fitting gives biased results. We rectify that omission here, by devising our own algorithm for fitting streams to positional and velocity data and – after testing and validation – we apply it to the GD-1 stream. This stream is a particularly attractive choice for probing the Galactic potential due to its unique 6-D dataset.

When studying the creation and evolution of tidal streams, an obvious tool is full N-body simulations. However, if we wish to explore parameter space for both the potential and the progenitor’s orbit, N-body methods are too computationally intensive (e.g., Fardal et al. 2012). Our first task is to find a rapid method of producing streams for fitting to data. Here, we take advantage of the fact that the majority of stars are stripped from near the satellite’s Lagrange points. Once generated, clouds of stripped stars are evolved forwards as test particles in the underlying potential of the satellite and host galaxy. This basic idea has been invoked in a number of recent works on tidal tail evolution (e.g., Varghese, Ibata & Lewis 2011, Küpper, Lane & Heggie 2012, Gibbons, Belokurov & Evans 2014). We use it here to repeat the work of K10 *without the simplifying assumption that the stream delineates an orbit*. We can therefore quantify the dangers of orbit fitting in a specific and practical case.

The paper is arranged as follows. In Section 2, we describe the Lagrange point stripping method used to create tidal streams. Section 3 describes how such streams can be compared to observational data. In Section 4, we validate the method by fitting to a stream produced using N-body simulations. Finally, in Section 5 we apply our stream fitting algorithm to the GD-1 stream and compare with the earlier orbit fitting results of K10.

## 2 STREAM CREATION BY LAGRANGE POINT STRIPPING

The computational cost of N-body simulations of a tidal stream formation lies in the calculation of the force between all the particles within the disrupting progenitor, particularly for smaller objects which have dynamical timescales orders of magnitudes smaller than their orbital periods. However, we are primarily interested in the stars which escape from the satellite and form the tails. A number of recent studies have shown that a convenient shortcut is to follow only the orbits of stars escaping through the two Lagrange points (see e.g., Küpper et al 2012).

The method used in this paper is broadly similar to, and was developed in conjunction with, the work of Gibbons et al. (2014, hereafter G14), where a more detailed explanation of some of the dynamical motivations can be found. Clouds of particles are released from the satellite at or around the Lagrange points, and their orbits integrated forward in the potential of both the host galaxy and the satellite. We evaluate the Lagrange radius as

$$r_t = \left( \frac{GM_{\text{sat}}}{\Omega^2 - \frac{d^2\Phi}{dr^2}} \right)^{\frac{1}{3}}, \quad (1)$$

where  $\Omega$  is the satellite’s angular velocity and  $\Phi$  is the halo potential. For this calculation of the Lagrange points, the satellite is approximated as a point mass. Stars are stripped from both the inner and outer Lagrange points at Galactocentric radii

$$r_{\text{strip}} = r_{\text{sat}} - \lambda r_t \quad \text{or} \quad r_{\text{sat}} + \lambda r_t, \quad (2)$$

where  $\lambda$  of order unity and  $r_{\text{sat}}$  is the instantaneous position of the satellite’s centre. If  $\lambda = 1$  (exact Lagrange point stripping, as used in G14), we find that a substantial number of the generated stars are re-captured by the satellite. This is particularly problematic just after pericentre, when the tidal radius of the satellite is growing rapidly. As we are only interested in escaping stars, this is computationally inefficient. For the purposes of the model, we use a value of  $\lambda = 1.2$ , which ensures that the overwhelming majority of the stars become part of the stream.

With the starting positions of the stripped stars in hand, they must be assigned velocities. The base velocity is determined by the orbit of the satellite, with the radial component matched directly to the satellite’s. For the tangential component, there are two obvious extremes – we can match either the satellite’s velocity (the choice made in G14) or its angular velocity. We find that the different choices have only a modest effect on the mean track of the stream over a range of masses. We choose to match to the angular velocity halfway between the satellite and the Lagrange point. This is similar to the method described in Küpper et al.(2012), and successfully reproduces streams from simulations. We add a random component to the velocities, described by a parameter  $\sigma_s$  which represents the satellite’s velocity dispersion. Three components resolved with respect to the progenitor’s orbital plane ( $v_r, v_t, v_\perp$ ) are drawn randomly from a normal distribution with zero mean and standard deviation  $\sigma_s$ .

As a satellite approaches perigalacticon, its tidal radius shrinks as the effect of the host galaxy grows. Conversely, at apocentre the tidal radius is at its largest. Consequently, the stripping of debris from a disrupting satellite is not uniform in time. N-body simulations show that whilst stars are stripped throughout the orbit, an excess is lost near pericentre. This is one of the factors controlling the density distribution along the stream. Others include the density distribution of the progenitor, the epicyclic motion of stars along the stream (e.g., Küpper et al. 2012) and any possible in-

interactions with other structures such as dark matter subhaloes. To sidestep this problem, we choose to fit only the mean track of the stream. This simplifies the problem greatly, and allows us to strip stars uniformly in time.

The orbits of the stripped stars are then integrated in the potential of the satellite and the host galaxy, producing a model tidal stream. Throughout this paper, we take the satellite potential to be a Plummer model, though different functional forms can easily be used. The algorithm used is the standard Runge-Kutta-Fehlberg method with an adaptive step size (e.g., Press et al. 2007). Relative and absolute error tolerances were set to  $10^{-5}$ , providing a reasonable trade-off between speed and accuracy. Generally, the age of a tidal stream is not well known, leaving us with the question of how long the stripping process should continue. We therefore also add a parameter  $t_d$ , the disruption time, determining how long ago the first star was stripped.

To establish confidence in our stream generation method, Fig. 1 shows a comparison of streams produced using the Lagrange point stripping model with an N-body simulation, using the freely available tree code GADGET-2 (Springel 2005). The model stream from the Lagrange point stripping method is virtually indistinguishable from the N-body stream.

In fitting, we model the data in a specific arm of the stream, and thus we wish to avoid contamination from particles which are either in the satellite or the wrong arm of the stream. However, not all of the stars stripped using this method become part of this stream. Some are recaptured by the satellite or escape into the other arm of the stream. Consequently, we remove any stars which do not escape the satellite, defined as stars which return to within a factor of 0.8 times the tidal radius at any time during their orbit integration. In practice, this tends to be roughly a quarter of the stars we generate.

### 3 THE MECHANICS OF FITTING

#### 3.1 Preliminaries

First, the model stream stars are converted from Cartesian coordinates to observables, namely angular position on the sky ( $\phi_1, \phi_2$ ), heliocentric distance  $d$ , line-of-sight velocity  $v_{los}$  and proper motion ( $\mu_{\phi_1}, \mu_{\phi_2}$ ). For this purpose, we assume that the Solar motion is represented by the circular orbit given by the Galaxy potential at the Solar radius of 8.5 kpc, together with a correction term for the Solar peculiar motion of (10.0, 5.25, 7.17)  $\text{kms}^{-1}$  (Dehnen & Binney 1998). This matches the values from K10, who used GD-1 to constrain Milky Way parameters via an orbit fitting method. This makes sense, as our purpose is to make a direct comparison between the two techniques.

Second, we restrict ourselves to simulations that actually produce a stream. The release of clouds of particles from the satellite's Lagrange points does not guarantee a stream. Highly radial satellite orbits, for example, produce shells and 'umbrellas' (e.g., Amorisco 2014). Similarly, individual stars with particularly unusual random initial conditions may not become stream members. An example of this is when stars undergo an energetic three-body interaction with the host galaxy and progenitor satellite. Tidal streams are formed from stars with energies and angular momenta close to that of the progenitor satellite; certain types of interaction lead to a dramatic change in these properties, permitting stars to escape onto highly energetic trajectories and to be flung to distant parts of the galaxy. We find that it is sufficient to make a simple cut in position in order to remove such stars; we therefore first sort the particles in the

stream by their angle along it  $\phi_1$ . Having sorted the stream particles by angle, we remove the outlying 2% at either edge. This eliminates the presence of contaminants and removes the poorly sampled edges of the stream.

When we compare model and data, we extract a segment of the stream which covers the angular extent of the observations. If the model does not cover the entirety of this extent, or if there are very few stars in this region, we can instantly reject the model. However, we do not wish to have sharp spikes in the likelihood function where the returned value changes instantly to zero, as this makes the parameter space more difficult to explore. It is useful to let the walkers know they are in the right region, even if the stream does not quite cover the extent of the data. We therefore introduce a weight function which allows the likelihood value to smoothly decrease to zero. The returned log-likelihood (always negative, see Section 3.3) is divided by a weight between zero and one (zero if the range of the stream is not covered, one if it extends more than  $5^\circ$  further). The weight varies linearly within this  $5^\circ$  regime. We wish the model stream to cover a greater range than our data points for two reasons. First, the extent of the data points does not represent the extent of the observations, as the data points come from binned photometric data (for simulated streams, we can select a segment we know extends at least  $5^\circ$  further. Secondly, the stream density for the model stream on average decreases as distance from the progenitor increases; therefore, some of the model stream we expect to be undetectable in observations.

#### 3.2 The stream track

We chose to fit the data using the centroids of the model stream in observable coordinates as a function of angle along the stream  $\phi_1$ . This is in distinction to Sanders & Binney (2013a,b) and Bovy (2014), who describe methods in action-angle space of producing a probability distribution function for model streams. We find that the technique described here of using only the mean track of the stream is sufficient to model data of the current quality.

The Lagrange point stripping method produces an adjustable number, roughly between 500–1000, of tracer particles which map the stream. To define the stream centroid for each of the coordinates along the stream, we must solve the familiar problem of how best to fit a line through a subset of points. For this purpose, we use a quadratic spline, but questions arise such as how much (if at all) we should bin the model stream particles and how smooth the curves we fit should be.

The eventual method was determined heuristically, after exploring a number of possible options. We bin the model stars for two main reasons. First, most of the parameters are observationally determined from photometric data, which are already pixellated. Second, binning serves to reduce the random noise or 'bumpiness' in the likelihood function. In general, a small change in the initial model parameters should lead to a small change in the returned likelihood. A smooth likelihood surface is easier for both gradient descent and Monte Carlo methods to explore effectively. However, the random generation of stars means that (even with fixed seeds) an infinitesimal parameter change can lead to a star becoming a stream member or not. This can cause curves fit directly to unbinned model particles to deviate sharply and unphysically.

Of course, the trouble with binning is that information about the curvature within each bin is necessarily lost. Some of the observed coordinates can vary reasonably steeply across a bin in certain circumstances. We can mitigate this by using a coordinate system defined by the stream itself, in which this curvature is mini-

Parameter	Description
$v_0, q$	Potential parameters
$R, z$	Progenitor position
$v_R, v_\phi, v_z$	Progenitor velocity
$M_s, a_s, \sigma_s$	Progenitor properties
$t_d$	Disruption timescale

**Table 1.** Table displaying the parameters for a full stream model. We can fix the angular position  $\theta$  without loss of generality.

mized. We do this by fitting a smooth quadratic spline through the *data* for each of the observables as a function of  $\phi_1$ . These curves are subtracted from the model stream’s observable co-ordinates, creating a new ‘stream-like’ coordinate system. The model curve fitting is then performed in these coordinates which have naturally reduced curvature, thus minimizing any deviations caused by the curve fitting.

The bin sizes are determined according to two criteria. We require that there are a minimum number of 10 stars per bin. This gives us a large enough statistical sample that we reduce the above effect, and prevent small number statistics leading to outlying points. We also set a minimum bin size of 0.1 radians. This avoids the oversampling of high density regions of the stream, which can lead to unphysically rapid oscillations in the mean track.

Once the bins have been determined, we can evaluate the mean values of the observables,  $\phi_2, d, v_{\text{los}}, \mu_{\phi_1}$  and  $\mu_{\phi_2}$ , as a function of angle along the stream. An unsmoothed quadratic spline is then fit through the mean positions using the inbuilt Python SciPy libraries. The spline is unsmoothed as the binning process already provides smoothing. A quadratic spline is then easily sufficient to describe the data’s curvature.

### 3.3 The likelihood value

The next step is to devise a metric by which the simulated data can be compared with the observations. The splines representing the model define the stream centroid at any point along the stream. As the curves pass through the observations, we can use the errors on the data to provide a  $\chi^2$  value for the fit. The log-likelihood function is thus

$$\ln \mathcal{L} = -\frac{\chi^2}{2} = -\sum_i \frac{(x_{\text{model},i} - x_{\text{data},i})^2}{2\sigma_i^2}, \quad (3)$$

where  $x_i$  is each of the observables and  $\sigma_i$  the associated error.

### 3.4 Parameter Exploration

A popular method of exploring a large parameter space is using Markov chain Monte Carlo (MCMC) methods. When given an a likelihood function, these permit a fully probabilistic determination of the posterior distribution. The premise is that a large number of ‘walkers’ are placed in some distribution within the parameter space we wish to explore. They move around the space according to some prescription, which in this case is a function of the locations of the other walkers in the ensemble. The value of the likelihood function at the new location is then compared to the original position; if the likelihood is greater, the walker moves to the new location. If it is less, it moves with some probability. It can be mathematically proved that after an infinite number of steps the distribution of walkers represents the posterior distribution. In practice, we consider the MCMC chain to be converged once the distribution of

walkers is no longer changing significantly. As this is a probabilistic process, appropriate priors on distributions of parameters can be included. The code we use is a modified version of the open source EMCEE (Foreman-Mackey et al. 2013). The modifications allow us to store arbitrary metadata (such as the current progenitor position for the most likely stream candidate) from the likelihood calls.

Standard MCMC algorithms do not necessarily deal well with multi-modal or complex likelihood contours (e.g., Feroz & Hobson 2008). The primary source of this is the unavoidable discretizations in the model. For example, we only sample a finite number of epochs, and the model stream only contains a finite number of stars. Another source of bumpiness in the likelihood surface is the procedure of fitting splines through the stars in the model stream. Whilst we have attempted to minimize deviations in the fitting process, we still find that small changes in the positions of the stars can still lead to significant changes in the spline fits. This translates to an uncertainty in the model, causing random noise on small scales in the returned likelihood. This in turn means small parameter variations can lead to larger than desired changes in the likelihood value. We find that the EMCEE code’s built in parallel tempering sampler helps us navigate this issue. This works via the concurrent running of MCMC chains at higher temperatures and allowing walkers to move between chains. These higher temperature chains have larger step sizes and accept distant points more frequently, allowing safe navigation of the ‘bumps’. This helps prevent walkers becoming stuck in local minima.

Whilst the small-scale ‘bumpiness’ can be dealt with, it unavoidably leads to relatively low acceptance fractions. These are of order 10% in the lowest temperature chain. As a consequence, chains can take a relatively large number of steps to converge. One simple test to assess convergence is look at the mean likelihood value in the chain on a step by step basis. If this is still changing, we can guarantee the chain has not converged, though the converse is not true. Once the mean likelihood value in the chain has reached a constant, we examine convergence by assessing whether the posteriors are changing, comparing them for two subsets of walkers in the chain. For example, if there are 4000 steps, and the posteriors in the steps 3001 – 3500 are the same as those within 3501 – 4000, we expect the chain to have converged. Another test of convergence is the Gelman and Rubin (1992) diagnostic, which is a technique based on the within-chain and between-chain variance for a number of MCMC chains. This allows us to evaluate the potential scale reduction factor, a statistic that is expected to be close to unity for a converged chain. We find that for all of our sample runs and our analysis of the GD-1 stream, this factor is within 0.5% of unity ( $< 1.005$ ).

When performing our parameter exploration, we use 2048 walkers split evenly between four temperatures. The temperature ladder scales exponentially, with each temperature increasing by a factor of  $\sqrt{2}$ . The EMCEE code implements ‘one temperature swap proposal per walker per rung on the temperature ladder after each ensemble update’. The chains are run for a total of 4000 steps (over 8 million individual likelihood calls). We consider the first 3000 of these steps to be our burn-in period, leaving a final lowest temperature chain with around five hundred thousand steps. If there were reason to believe that the chains had not converged, then the burn-in period could be extended. However this has not proved necessary in any case thus far.

Theoretically, our complete parameter space for a full MCMC run consists of the potential parameters, six satellite phase space coordinates for the progenitor position, and four parameters giving the satellite mass, size, velocity dispersion and disruption timescale



(see Table 1). We can however reduce this dimensionality by one by taking advantage of the fact that when we produce a stream, we do not only compute its final configuration. Instead, we can store the positions of the stars in the stream at a number of different snapshots. We do this at 500 equally spaced timesteps throughout the disruption timescale  $t_d$ . We therefore do not require six parameters for the satellite phase space position and a timescale; instead, a satellite orbit can be defined by five varying MCMC parameters and one fixed co-ordinate. The likelihood function described in the previous section can then be evaluated at the various stored epochs. As the epoch varies, so evidently does the satellite position, meaning our ‘fixed’ coordinate does not in fact remain the same for each likelihood call.

The coordinate we choose to fix is the azimuthal angle,  $\theta = \theta_f$ . We choose  $\theta_f$  such that the progenitor passes through  $\theta_f$  in the near future. For example, for a leading stream we choose  $\theta_f$  to be at the edge of the stream, as we know the progenitor will imminently pass through this angle. Consequently, when the satellite orbit is integrated backwards and the stream produced, we can guarantee that the ‘correct’ epoch (the satellite’s present day position) will be included.

In general, our disruption timescale consists of a large number of satellite angular periods, and thus the present day  $\theta$  value of the progenitor occurs a number of times. In theory, we can therefore find that the stream fits the data well at a late snapshot (the most recent wrap of the orbit), or a much earlier snapshot corresponding to an earlier angular passage. This means that we artificially introduce a multi-modality into our MCMC posterior for our fixed  $\theta_f$ , corresponding to the remaining five phase space co-ordinates of the orbit. These five parameters are different for a fixed  $\theta_f$  on subsequent wraps of the orbit, introducing a degeneracy despite the fact they correspond to the same satellite orbit and thus the same solution. When we integrate backwards from these co-ordinates, we find a stream which fits the data regardless of whether it was on the most recent wrap. As multi-modal posteriors are more difficult to explore, we wish to prevent this happening. Consequently, we do not evaluate our likelihood function at every snapshot. Instead, we only extract the most recent ‘wrap’, such that the range of progenitor positions covers no more than  $2\pi$ .

After the likelihood is calculated for these snapshots, we perform a zoom-in about the best epoch, interpolating the position of each star in the stream at 200 evenly spaced times between the epoch prior to and immediately after the best epoch. The best fit of this zoom-in is returned as the likelihood value of the fit. Theoretically, we should in fact marginalize over all the likelihood evaluations at the different timesteps for each evaluation in our MCMC. However, in practice we find that the likelihood very sharply peaked in time. Combined with the fact that the width of this peak remains consistent for similar orbits, it can be well modelled by a delta function, meaning taking the best value is approximately equivalent to marginalization.

#### 4 A SAMPLE FIT

In order to test the entire algorithm, we simulate a tidal stream with GADGET and try to recover potential parameters. For this case, we used the correct functional form of the potential and assume knowledge of properties (the size and mass) of the progenitor.

We produced a tidal stream via an N-body disruption of a Plummer satellite orbiting in a fixed logarithmic potential of the

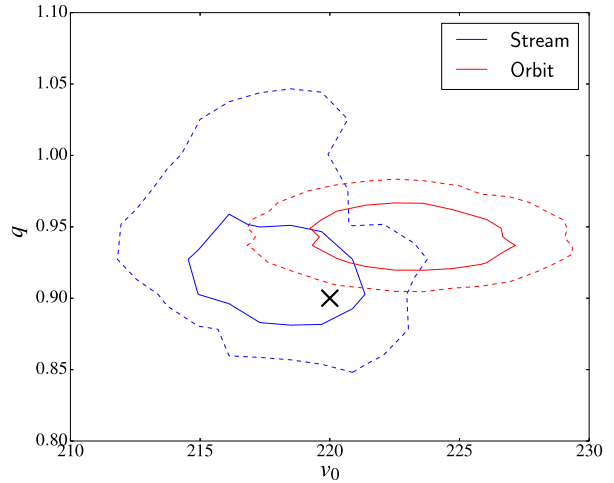


**Figure 2.** Contour plot showing the posterior probability distribution of potential parameters for a fit to a stream produced from an N-body simulation. The black cross shows the true values. The stream fit is shown in blue and the orbit fit in red, with the solid lines representing  $1\sigma$  contours and the dashed lines  $2\sigma$ . For the stream fit, the recovered parameters are within  $1\sigma$  of the correct value. The orbit fit recovers a flattening inconsistent at the  $2\sigma$  level with the correct value.

form (e.g., Binney & Tremaine 1987)

$$\Phi(R, z) = \frac{v_0^2}{2} \ln \left( R^2 + \frac{z^2}{q^2} \right), \quad (4)$$

with  $v_0 = 220.0 \text{ km s}^{-1}$  and  $q = 0.9$ . A satellite of mass  $2.5 \times 10^5 M_\odot$  was placed on an orbit beginning at  $(x, y, z, v_x, v_y, v_z)$  given by  $(26.0, 0.0, 0.0, 0.0, -141.8, 83.1)$  in units of  $\text{km s}^{-1}$  and kpc. The positions and velocities of the particles in the satellite were drawn from a Plummer sphere with scale radius  $a$  of 8 pc. The simulation was evolved for 10 Gyr.

Simulation data are first converted to observational ‘data’ for a stream roughly 6.5 Gyrs old. We extract an angular segment of the stream corresponding to the range we wish the fake ‘data’ to cover. The stars in this segment are then sorted by angle along the stream. Their Cartesian coordinates are transformed into observables  $(\phi_1, \phi_2, d, v_{\text{los}}, \mu_{\phi_1}, \mu_{\phi_2})$ , using the solar position, Local Standard of Rest and solar peculiar velocity. We then binned the stars in 10 evenly spaced bins in  $\phi_1$ , the angle along the stream, and took the means of the other observables in these bins as the data. Gaussian noise was added to each value, with the error for each point taken as the standard deviation of the Gaussian. These standard deviations for the coordinates  $(\phi_2/\text{rad}, d/\text{kpc}, v_r/\text{km s}^{-1}, \mu_{\phi_1}/\text{mas yr}^{-1}, \mu_{\phi_2}/\text{mas yr}^{-1})$  were given by  $(0.005, 0.25, 2.5, 0.125, 0.125)$ . With the exception of the  $\phi_2$  coordinate, these values are overly optimistic for current data.

We fit this stream using the model described in Sections 2 and 3, extracting the potential parameters. The results of the fit are shown in blue in Fig. 2, with solid and dashed lines showing one and two sigma contours. The recovered potential parameters are  $v_0 = 218.0^{+2.1}_{-1.6} \text{ km s}^{-1}$  and  $q = 0.921^{+0.017}_{-0.024}$ , within  $1\sigma$  of the correct values as marked by the black cross. We can compare this to the result of orbit fitting to the same data, shown in the red in Fig. 2. The recovered potential parameters are  $v_0 = 223.1^{+2.3}_{-2.6} \text{ km s}^{-1}$  and  $q = 0.943^{+0.012}_{-0.018}$ . This plot does show the superiority of stream fitting,

Parameter			
5	≤	$R/\text{kpc}$	≤ 35
−30	≤	$z/\text{kpc}$	≤ 30
−100	≤	$v_R/\text{kms}^{-1}$	≤ 200
−50	≤	$v_\phi/\text{kms}^{-1}$	≤ 350
−200	≤	$v_z/\text{kms}^{-1}$	≤ 0
130	≤	$v_0/\text{kms}^{-1}$	≤ 290
0.5	≤	$q$	≤ 1.5
4.5	≤	$\log(M_s/M_\odot)$	≤ 5.5
−3	≤	$\log(a_s/\text{kpc})$	≤ −2
0.5	≤	$\sigma_s/\text{kms}^{-1}$	≤ 2.5
2	≤	$t_d/\text{kpckm}^{-1}\text{s}$	≤ 5

**Table 2.** Table displaying the uniform model priors for the leading and trailing fits to GD-1 stream.

as the recovered parameters are recovered more closely. The likelihood contours are slightly offset from the true value due to the noise added to the fake observations of the stream. The orbit fit is slightly worse, and the axis ratio is now no longer consistent at the  $2\sigma$  level with the correct value. However, it is worth noting that the likelihood ( $\chi^2$ ) values returned by the two models are very similar – the stream can be well fit by an orbit, just not an orbit in the correct potential (which for this idealised experiment we know).

## 5 THE GD-1 STREAM

We now apply the algorithm described in Sections 2 and 3 to real observations in an effort to place constraints on the potential of the Milky Way. The stream we use is GD-1 (Grillmair & Dionatos 2006). Its length, spanning  $60^\circ$  on the sky, as well as its relative coldness make it an excellent target. Its biggest failing is the limited range of distances it spans. The stream data are confined to Galactocentric radii between 11.5 and 13.5 kpc, and to heights between 4 and 8.5 kpc above the Galactic plane.

The GD-1 data is described in full in K10, where an orbit fitting method is used to probe the Galactic potential. It consists of 6-D data along the stream – positions, distances and proper motions are determined from photometric data from SDSS. Radial velocities are from a combination of binned SDSS data and observations of individual stars from the Calar Alto observatory. Observations of the density distribution along the stream are limited, so whether the stream is leading or trailing (or both) is unknown, as is the location of the progenitor. We will therefore perform two different fits, assuming a leading stream and a trailing stream separately.

For the fitting, we start with wide-ranging uniform priors described in Table 2. The five phase space priors are sufficiently broad to guarantee, given the properties of the stream, that the satellite orbit is well within their range. Similarly, we can expect the potential normalization and flattening to lie within the bounds we have given. We cannot make the same statement for the satellite properties, as we know little about GD-1’s progenitor. However, for a kinematically cold stream like GD-1, the nature of the progenitor plays a relatively small role in the track of the stream, thus we can achieve good fits with a broad range of values for  $M_s$  and  $a_s$ . Similarly, it is difficult from the observations to constrain the age of the stream, so we chose a timescale for the disruption that produces a stream of roughly the correct length.

The results of the fitting are shown in Fig. 3. The green contours assume the data are from the trailing arm, the blue from the leading arm, and the red contours show an orbit fit. Solid lines rep-

resent  $1\sigma$  contours, whilst dashed lines are  $2\sigma$ . The trailing stream fit recovers parameters of  $v_0 = 226.5^{+17.9}_{-17.0} \text{ kms}^{-1}$ ,  $q = 0.903^{+0.049}_{-0.093}$ . The leading fit recovers  $v_0 = 227.2^{+15.6}_{-18.2} \text{ kms}^{-1}$ ,  $q = 0.908^{+0.043}_{-0.113}$ . The orbit fit returns  $v_0 = 228.3^{+12.3}_{-12.2} \text{ kms}^{-1}$ ,  $q = 0.856^{+0.023}_{-0.051}$ . It is interesting to note that these values are slightly different to those recovered by the orbit fit in K10, namely  $v_0 = 224 \pm 13 \text{ kms}^{-1}$  and  $q = 0.87^{+0.07}_{-0.04}$ , though they are consistent to within  $1\sigma$ . This is plausibly due to the differing methodologies used for the fitting. As visual confirmation that the fits are good, we also show the fit to the leading stream in the space of observables in the same figure. In Fig. 6 we provide an example of a leading stream fit with the positions and velocities of the test particles and the present location of the satellite displayed.

Our fits do not provide strong constraints on the satellite properties. Posteriors for these values are shown in the panels of Fig. 4. Both fits show almost entirely flat posteriors for the satellite mass  $M_s$  and lengthscale  $a_s$ . There is some evidence for a slight drop off towards higher values of the velocity dispersion  $\sigma_s$ . In both cases, the disruption time is flat towards the higher end, dropping off at lower disruption times.

We also show our constraints on the orbital properties of the GD-1 progenitor in Fig. 5, displaying the previous and next pericentre distances, the intervening apocentre distance, and the time between the two pericentric passages. It should be noted that in a flattened potential this period is not constant between subsequent passages. The recovered posteriors are very similar between leading and trailing fits, with the only discrepancy being the closeness of the next pericentric approach, which is slightly nearer the centre for a trailing stream. We observe that the stream is currently very near pericentre; this is as we would expect from its extended, thin nature. If it were near apocentre, we would expect more clumping of the stars. The range of apocentres and periods are reasonably large, spanning 15 – 40 kpc and 250 – 600 Myr respectively. It is not clear how well constrained these parameters are – the nature of the stream at pericentre is not necessarily affected strongly by the properties of the orbit at larger distances. The recovered apocentre and period values could change dramatically if our assumed functional logarithmic form changes at larger radii.

We observe that stream fitting is consistent at the  $1\sigma$  level with orbit fitting. There are some systematic – but slight – offsets. Nonetheless, the agreement is impressive, especially given the underlying simplicity of the assumption that an orbit is a stream. Of course, this does not imply that orbit fitting is without dangers. However, it does vindicate the work of K10 given the quality of the current data. We have demonstrated that – for present observations of a kinematically cold stream in the outer parts of the Galaxy represented by an axisymmetric logarithmic potential – no serious problems do arise when the orbit approximation is used.

Sanders & Binney (2013a) showed that a stream can only be successfully modelled as an orbit if the misalignment angle is small. This angle is given by

$$\varphi = \arccos(\hat{\Omega} \cdot \hat{e}_1), \quad (5)$$

where  $\hat{\Omega}$  is the normalised frequency vector of the progenitor of the stellar stream and  $\hat{e}_1$  is the leading eigenvector of the Hessian matrix of the Hamiltonian with respect to the actions, viz.

$$D_{ij}(J) = \frac{\partial^2 H}{\partial J_i \partial J_j}. \quad (6)$$

However, Hamiltonians of scale-free spherical logarithmic potentials are linear in the actions to a very good approximation (e.g., Williams, Evans & Bowden 2014) and so the misalignment an-

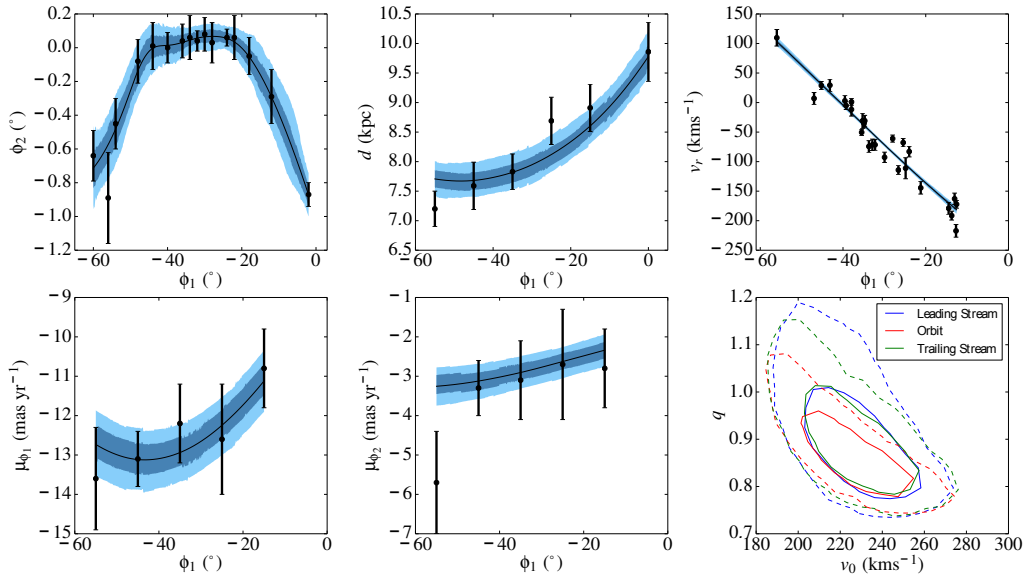


**Figure 3.** Results for fitting GD-1. The bottom right panel shows the recovered posterior probability distribution of potential parameters for the GD-1 stream. Green, blue and red lines show a trailing stream fit, leading stream fit and orbit fit respectively, with the solid lines representing  $1\sigma$  contours and the dashed lines  $2\sigma$ . The remaining five panels show an aggregation of 10,000 randomly selected leading stream fits from the post burn-in MCMC chain - the trailing stream and orbit fits are of a very similar quality. The dark blue shaded regions cover 68.3% of the models, and the light blue 95.5%. The models provide a good fit to the data in all observable co-ordinates.

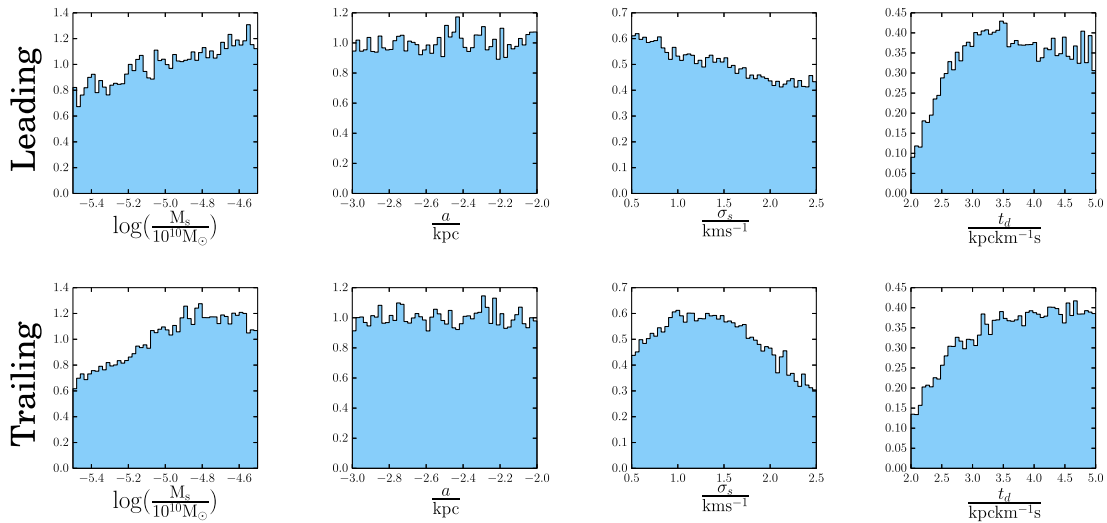


**Figure 4.** Posterior distributions on the satellite properties for leading (upper) and trailing (lower) stream fit to the GD-1 data. The only real constraining statement that can be made is that very short disruption times are disfavoured.

gle almost vanishes. The excellent performance of orbit fitting may therefore be a consequence of the assumed form for the potential, and it may not hold for more elaborate models in which the Hamiltonian has a more complicated dependence on the actions.

The choice of a flattened logarithmic potential was primarily motivated by the desire to perform a direct comparison with the results of K10. Although this functional form is simple, it is a reasonable approximation to the total Galactic potential, at least well

away from the disk. The fitting is sensitive to the force components along the stream. This means the constraints on the flattening and normalization are at best valid in a narrow regime at a distance of  $\sim 15$  kpc from the Galactic Centre. Fitting GD-1 data certainly does not constrain the global flattening, or the overall shape or normalisation of the Galactic rotation curve,

In both leading and trailing stream cases, the recovered posteriors are just barely consistent at the  $1\sigma$  level with a spherical

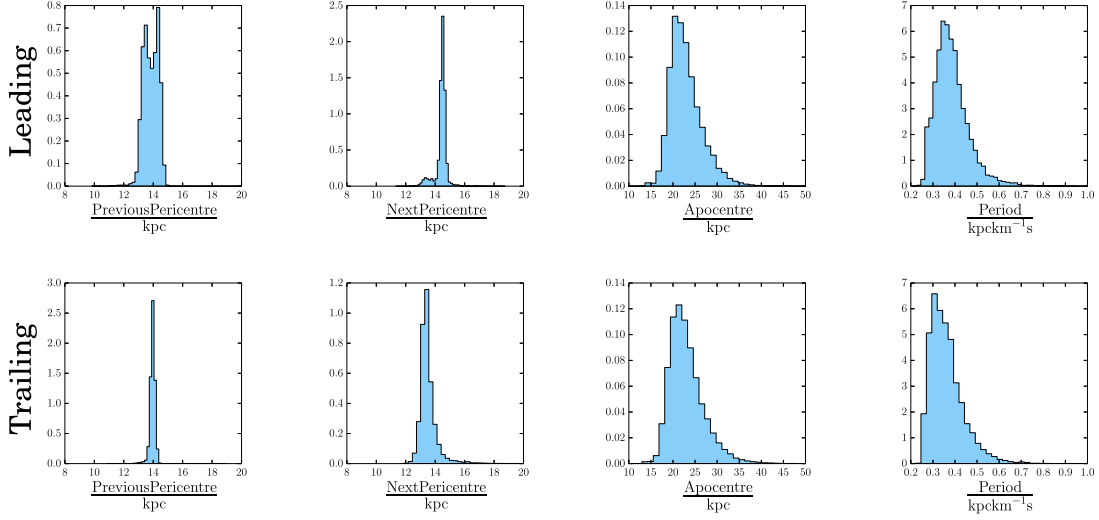


**Figure 5.** Posterior distributions on the orbital properties for the GD-1 satellite under the assumption of a leading (upper) and trailing (lower) stream fit. The previous and next pericentric passage distance are displayed, along with the intervening apocentre. The period described here is the length of time between these two pericentres; this is not a constant value as the halo is not spherical.

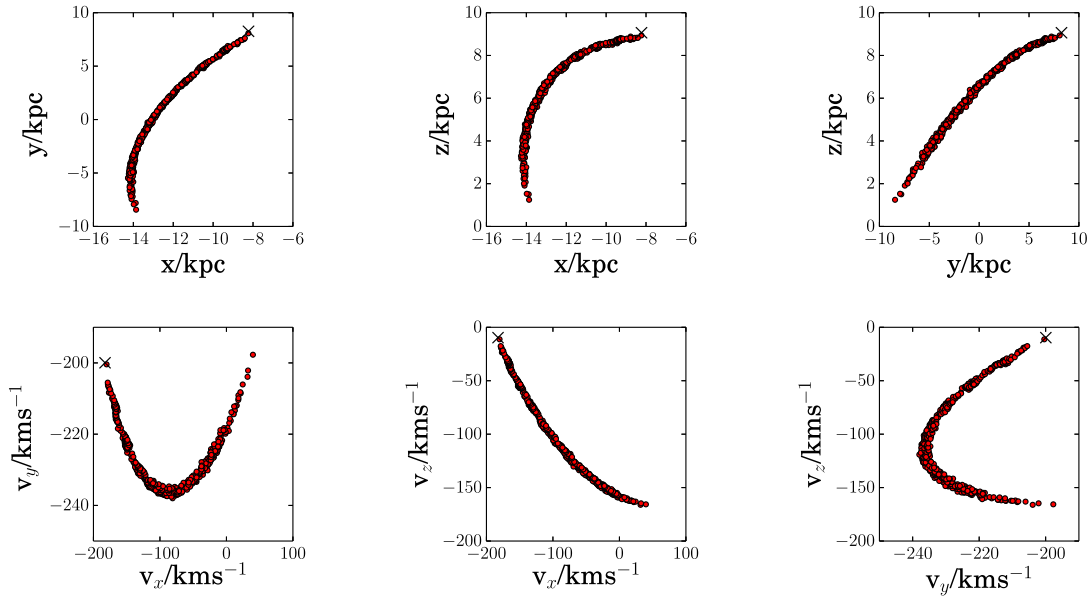


**Figure 6.** Positions and velocities for the test particles in a model stream. The black cross shows the current position of the progenitor in this model. The fit was for a leading stream, performed in a potential with  $v_0 = 241.6 \text{ km s}^{-1}$ ,  $q = 0.829$ .

potential ( $q = 1$ ). Whilst the GD-1 stream provides evidence pointing towards a flattened potential, this is expected given its location relative to the disk. At its closest point, the stream is 4.5 kpc above the Galactic plane. Given the disk flattens the global potential anyhow, it is evident that near-spherical halos, or even spherical haloes, are not ruled out. The axis ratio in the density contours  $q_\rho$  is related to the flattening in the potential by (see eq 2.2 of Evans 1993)

$$q_\rho = q \sqrt{2q^2 - 1} \quad (7)$$

The density contours are always flatter than the potential contours, unless  $q = 1$ . A flattening in the potential of  $q = 0.8$  corresponds to an axis ratio in the density of  $q_\rho = 0.42$ , and so the  $1\sigma$  contours are also consistent with a substantial range of flattenings. However, the GD-1 stream does confirm that the halo potential cannot be very highly flattened at these radii, which is consistent with results from the Sagittarius stream (Evans & Bowden 2014).

In order to approximate the effect of including a disk in our potential model, we performed a simple test calculation. To esti-



mate the degree of flattening in the halo compared to the disk, we wished to compare a flattened logarithmic halo model to a flattened log halo plus disk. We therefore took a logarithmic halo with  $v_0 = 240.0 \text{ km s}^{-1}$ ,  $q = 0.85$  and calculated its R and z derivatives across a 2-D grid in (R,z). This grid spanned 11.5 – 13.5 kpc in R and 4.5 – 8.5 kpc in z, covering the location of the GD-1 stream. We then fit these derivatives with a disk and halo model with fixed disk parameters. Here, we took the disk to be a razor thin exponential disk with mass  $M_d = 6 \times 10^{10} M_\odot$  and scale radius  $a = 3 \text{ kpc}$ . The force components for the original potential - that which our stream model constrains - are best fit in this case by a halo component with  $v_0 = 200.0 \text{ km s}^{-1}$ ,  $q = 0.866$ . This suggests that such a razor thin exponential disk has a very mild effect on the flattening of the potential at the heights above the galactic plane occupied by GD-1.

In order to provide truly global constraints, we need to fit multiple streams at different radii to probe more of the Galaxy. There is scope for the modelling and the parameter estimation that we have developed here to play a major role. Computational speed is not an issue for our algorithm, with a single likelihood call generating a stream taking of the order of a few seconds. Using modest computational resources, this allows us to fully fit a stream on the timescale of a week by exploring many models. For comparison, a single N-body simulation using GADGET carried out on a single core (as the model is) would take of the order of a week. However, fitting multiple streams – possibly with other data such as the HI rotation curve and the Oort’s constants – requires a much more flexible model of the Galaxy’s potential than has hitherto been developed. The complicated effects of realistic halos, including perturbations from dark sub-halos and from nearby satellite galaxies, may also need to be accounted for.

## 6 CONCLUSIONS

We have carried out the first fitting of a model stream to 6-D data for tidal stream stars in the Galaxy with an algorithm that takes into account the fact that the stars follow a stream, and not an orbit. Orbit fitting has often been used before (e.g., Jin & Lynden-Bell 2007, Willet et al. 2010, Koposov et al. 2010, Newberg et al. 2011). In recent years, the practice has fallen into abeyance, with a number of authors suggesting it may give misleading or even dangerous results (e.g., Binney 2008, Sanders & Binney 2013a,b, Bovy 2014). However, a practical example of the likely biases based on data on an actual stream in the Galaxy has been missing from the literature.

Streams are produced by the stripping of stars from the Lagrange points of disrupting satellites. This can be routinely followed by N-body simulations, though this is too slow for proper exploration of parameter space. Accordingly, we use a method that quickly produces streams via the release of stars from Lagrange points and subsequent integration of their orbits in the potential of the Galaxy and progenitor (c.f. Varghese et al 2011, Küpper et al. 2012). Recently, Gibbons et al. (2014, hereafter G14) used a very similar method to study the apocentric precession in the Sagittarius stream and to infer the Milky Way mass. However, this paper provides the first direct modelling of stream observations assuming they are indeed a stream.

Our method is applied to the GD-1 stream, which was discovered by Grillmair & Dionatos (2006) in Sloan Digital Sky Survey data. It is a narrow arc of  $60^\circ$  on the sky at a distance of  $\sim 15 \text{ kpc}$  from the Galactic Centre. The observational data include positions on the sky, heliocentric distances, radial velocities and proper motions. The GD-1 stream has been fit before, but only under the sim-

plifying assumption that it follows an orbit (Koposov et al. 2010, hereafter K10). For this reason, we made the same assumption as K10 as regards the Galactic potential, taking it to be an axisymmetric logarithmic model characterised by an overall normalisation  $v_0$  and a flattening  $q$ . We can therefore directly compare the effects of stream fitting and orbit fitting and elucidate any biases.

When GD-1 is fit as a leading stream, we recover parameters of  $v_0 = 227.2^{+15.6}_{-18.2} \text{ km s}^{-1}$ ,  $q = 0.908^{+0.043}_{-0.113}$ . When it is fit as a trailing stream, recovered parameters are  $v_0 = 226.5^{+17.9}_{-17.0} \text{ km s}^{-1}$ ,  $q = 0.903^{+0.049}_{-0.093}$ . Both these fits are consistent at the  $1\sigma$  level with the orbit fitting method of K10, who obtained  $v_0 = 224 \pm 13 \text{ km s}^{-1}$  and  $q = 0.87^{+0.07}_{-0.04}$ . Although there are differences in the posterior parameter values, they are small. This therefore provides an explicit example showing that orbit fitting to streams can provide accurate results with current data – at least for kinematically cold streams in the outer Galaxy.

There are still reasons to be cautious about orbit fitting. The scale-free logarithmic potential used here and in K10 has a particularly simple Hamiltonian structure (Williams, Evans & Bowden 2014). This is relevant because the misalignment between the stream and the orbit is controlled by the Hessian of the Hamiltonian with respect to the actions (Sanders & Binney 2013a). It is reassuring that orbit fitting works so well with the commonly used logarithmic potential, but it may fail in more complex multi-component potentials, as suggested by Sanders & Binney (2013a). The inner Galaxy is more poorly represented by scale-free potentials, and so orbit fitting must remain highly suspect in this regime still.

Fits to a single stream do not constrain the global Galactic matter distribution, or the potential. What is constrained is the force components in the small region of phase space covered by the orbit. Fits to GD-1 do suggest that the overall potential is flattened at distances of  $\sim 15 \text{ kpc}$  from the Galactic Centre. The constraint on the flattening is actually quite weak. Spherical haloes are consistent with the result at the  $1\sigma$  level, especially given the fact that some of the measured flattening in the potential is due to the effects of the disk. However, the  $1\sigma$  contours are also consistent with substantial flattening in the density with axis ratios  $q_p \approx 0.4$ .

To improve the constraints necessitates the fitting of more streams. The fast stream production and fitting algorithm that we have developed, introduced here and in G14, can play an important role in multiple stream fitting. Before this can be made a practical tool to constrain the Galactic potential, two things are needed. First, observational data comparable to – or better still superior to – the quality and quantity available for GD-1 needs to be procured for many more streams. Second, the Galactic potential needs to be parametrised in a much more flexible way so that multiple constraints from different streams can be fit simultaneously. We plan to return to this problem in the near future.

## ACKNOWLEDGMENTS

AB thanks the Science and Technology Facilities Council (STFC) for the award of a studentship. We thank Simon Gibbons, Sergey Koposov and Denis Erkal for many useful comments and discussions on streams. The referee is thanked for a careful and constructive reading of the paper.

## REFERENCES

Amorisco N.C., 2014, MNRAS, submitted (arXiv 1410.0360)

- Belokurov V., Evans N.W., Irwin M.J., Hewett P.C. Wilkinson M.I., 2006, *ApJ*, 637, L29
- Belokurov V. et al., 2007, *ApJ*, 658, 337
- Belokurov V. et al., 2014, *ApJ*, 437, 116
- Binney J., 2008, *MNRAS*, 386, L47
- Binney J., Tremaine S. 1987, *Galactic Dynamics*, Princeton University Press
- Bonaca A., Geha M., Küpper A., Diemand J., Johnston K.V., Hogg D.W. 2014, *ApJ*, 795, 94
- Bovy J., 2014, *ApJ*, 795, 95
- Deg N., Widrow L. 2014, *MNRAS*, 439, 2678
- Dehnen W., Binney J. 1998, *MNRAS*, 298, 387
- Evans N.W., 1993, *MNRAS*, 260, 191
- Evans N.W., Bowden A., 2014, *MNRAS*, 443, 2
- Eyre A., Binney J. 2011, *MNRAS*, 413, 1852
- Fardal M.A., et al. 2012, *MNRAS*, 434, 2779
- Fellhauer M., et al. 2006, *ApJ*, 651, 167
- eroz f., Hobson M. 2008, *MNRAS*, 384, 449
- Foreman-Mackey D., Hogg D.W., Lang D., Goodman J., 2013, *PASP*, 125, 306
- Gelman A., Rubin D. B., 1992 *Statistical Science*, Vol. 7, No. 4, 457-511
- Gibbons S., Belokurov V., Evans N.W., 2014, *MNRAS*, 445, 3788 (arXiv 1406.2243)
- Grillmair C., Johnson R., 2006, *ApJ*, 639, L17
- Grillmair C., Dionatos O., 2006, *ApJ*, 643, L17
- Grillmair C., 2009, *ApJ*, 693, 118
- Jin S., Lynden-Bell D., 2007, *MNRAS*, 378, L64
- Johnston K.V., Spergel D.N., Hernquist L. 1995, *ApJ*, 451, 598
- Koposov S., Rix H.W., Hogg D.W. 2010, *ApJ*, 712, 260
- Koposov S., et al. 2011, *ApJ*, 750, 80
- Küpper A., Lane R., Heggie D.C. 2012, *MNRAS*, 420, 2700
- Lux H., Read J.I., Lake G., Johnston K.V. 2013, *MNRAS*, 436, 2386
- Newberg H.J., Willett B. Yanny B., Xu Y. 2010, *ApJ*, 711, 32
- Niederste-Ostholt M., Belokurov V., Evans N.W., Penarrubia J. 2010, *ApJ*, 712, 516
- Odenkirchen M., et al. 2001, *ApJ*, 548, L165
- Press W., Teukolsky S., Vetterling W., Flannery B. 2007, *Numerical Recipes*, CUP
- Price-Whelan A., Hogg D.W., Johnston K.V., Hendel D., 2014, *ApJ*, 794, 4
- Sanders J., Binney J.J. 2013a, *MNTRAS*, 433, 1813
- Sanders J., Binney J.J. 2013a, *MNTRAS*, 433, 1826
- Springel V. 2005, 364, 1105
- Varghese A., Ibata R., Lewis G.F., 2011, *MNRAS*, 417, 198
- Willet B.A., Newberg H.J., Zhang H., Yanny B., Beers T.C. 2009, *ApJ*, 697, 207
- Williams A.A., Evans N.W., Bowden A., 2014, *MNRAS*, 442, 1405